

Assembling Wormlike Micelles in Tubular Nanopores by Tuning Surfactant–Wall Interactions

Bhuvnesh Bharti,[†] Mengjun Xue,[†] Jens Meissner,[†] Viviana Cristiglio,[‡] and Gerhard H. Findenege^{*,†}

[†]Stranski Laboratorium, Institut für Chemie, Technische Universität Berlin, Strasse des 17. Juni 124, D-10623 Berlin, Germany

[‡]Large Scale Structures Group, Institut Laue Langevin, 6 rue Jules Horowitz, BP 156, F-38042 Grenoble, France

S Supporting Information

ABSTRACT: Threadlike molecular assemblies are excluded from narrow pores unless attractive interactions with the confining pore walls compensate for the loss of configurational entropy. Here we show that wormlike surfactant micelles can be assembled in the 8 nm tubular nanopores of SBA-15 silica by adjusting the surfactant–pore-wall interactions. The modulation of the interactions was achieved by coadsorption of a surface modifier that also provides control over the partitioning of wormlike aggregates between the bulk solution and the pore space. We anticipate that the concept of tuning the interactions with the pore wall will be applicable to a wide variety of self-assembling molecules and pores.

Molecular assemblies are strongly influenced by confinement in space. The constraints imposed by the bounding surfaces can induce new structures and open pathways to materials with unique properties.¹ This concept has been demonstrated for diblock copolymers (formed by two chemically different polymers joined together on one end), for which the microphase separation in cylindrical pores can lead to cylindrical or helical structures or concentric layers, depending on the size ratio of the two blocks and the repeat period of the block copolymer in relation to the pore size.^{2–4} Confinement-induced self-organization of block copolymers has been observed in pores with typical diameters of 100 nm, but simulation studies have reported similar phenomena for short-chain amphiphiles in systems with nanotubes having diameters of less than 10 nm.^{5,6} A cornucopia of polymorphic surfactant assembly structures, including single- and double-stranded wormlike or spiral micelles, was presented in a study by Arai et al.⁷ However, this study was focused on the self-assembly in an isolated pore and could not tell whether the confinement-induced aggregates also existed in equilibrium with a bulk solution.

It is well-established that wormlike micelles in many ways behave as *living polymers*.⁸ For a flexible or semiflexible chain, the number of possible configurations in confined space is smaller than in dilute solutions, resulting in a loss of configurational entropy. Accordingly, polymers avoid entering into pores with sizes less than their effective molecular diameter⁹ unless this entropy loss is balanced by attractive interactions with the pore walls. The influence of attractive and repulsive polymer–surface interactions on the partitioning of polymer chains between a pore and a reservoir has been

highlighted in a theoretical study by Freed et al.¹⁰ Experimental verification of these predictions is difficult because of notorious problems related to the equilibration of polymer configurations at interfaces. These problems can be avoided in studies of the partitioning of living polymers that are assembled from monomeric units inside the pores. Results for the partition coefficient of wormlike micelles may be pertinent for classical polymers because the partitioning equilibrium should be independent of the mechanism of transport between the reservoir and the pore space. With this motivation, we studied self-assembled structures of a surfactant in cylindrical pores with diameters of less than 10 nm. The surfactant in the pore space is in equilibrium with a bulk solution, where it forms extended wormlike micelles. We aimed to find out whether the formation of wormlike micelles in the pores, although entropically disfavored, could be induced by adjusting the interactions with the pore wall. As a sensitive and precise in situ method for modulating the interaction of the surfactant with the pore walls, we adopted coadsorption of a low-molecular-weight substance that competes with the surfactant for the same adsorption sites at the surface.

Micellar aggregates of the nonionic surfactant pentaethylene glycol monododecyl ether (C₁₂E₅) formed by adsorption from solution into the cylindrical pores of SBA-15 silica were examined in situ by small-angle neutron scattering (SANS). SBA-15 constitutes two-dimensionally (2D) ordered arrays of cylindrical pores of uniform size disposed parallel to each other and separated by thin silica walls.^{11,12} The pore size of SBA-15 (ca. 8 nm) is distinctly larger than the cross-sectional diameter of wormlike micelles of the surfactant C₁₂E₅ (ca. 5 nm). In preceding studies,^{13,14} it was found that this surfactant forms adsorbed patchy bilayers, indicating relatively strong interactions with the pore walls. To modulate this interaction and induce the formation of cylindrical micelles, a strongly adsorbed amino acid (lysine) was used as the surface modifier in the present work.¹⁵ Slurry samples of SBA-15 with the surfactant and lysine were studied by SANS using a H₂O/D₂O solvent mixture that matches the scattering length density of the silica matrix (see Experimental Details). Scattering from the slurry samples represents a sum of two contributions:^{13,14} Bragg scattering (I_{Bragg}) from the pore lattice, which provides information about the averaged radial concentration profile of surfactant in a pore, and diffuse scattering (I_{diff}), which depends on how the surfactant aggregates are distributed in the matrix.

Received: July 31, 2012

Published: August 28, 2012

Here we focused on the Bragg scattering term, which enabled us to discriminate between different structural scenarios of the radial distribution of surfactant in a pore. For an array of long cylindrical objects, I_{Bragg} is given by¹³

$$I_{\text{Bragg}}(q) = KS(q)P(q) \quad (1)$$

where $S(q)$ is the structure factor of the pore lattice, $P(q)$ is the form factor of a unit cell, and K is a constant. The spherically averaged structure factor of a 2D hexagonal lattice is given by $S(q) = q^{-2} \sum_{hk} m_{hk} S_{hk}(q)$, in which m_{hk} is the multiplicity factor of a reflection with Miller indices hk [$m_{hk} = 6$ for the (10), (11), and (20) reflections]. The Bragg peaks $S_{hk}(q)$ were modeled by Gaussian functions $S_{hk}(q) = a_{hk} \exp[-b(q - q_{hk})^2]$ located at positions $q_{hk} = (4\pi/a_0\sqrt{3})(h^2 + k^2 + hk)^{1/2}$, where a_0 is the lattice parameter of SBA-15, a_{hk} is the amplitude of peak (hk), and b characterizes the width of the Gaussian peaks, which was kept constant in the data analysis of all of the samples. The form factor $P(q)$ in eq 1 was modeled for different surfactant aggregate morphologies. Simulated Bragg scattering profiles for two different modes of surfactant self-assembly in the pore and for the case of micelle formation outside the pore space are shown in Figure 1. The simulations were based on the lattice

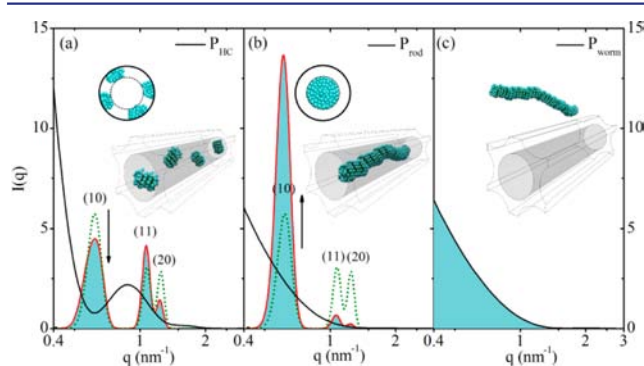


Figure 1. Simulated scattering profiles for three scenarios of surfactant aggregation as sketched in the cartoons (insets): (a) surface micelles adsorbed on the pore wall; (b) rodlike micelles in the core of the pore; (c) wormlike micelles in the solution outside the pores. The form factor of the aggregates is indicated by solid black lines, and the Bragg peaks for empty pores are shown as dotted lines; net scattering profiles for the three cases are indicated by the shaded areas.

parameter ($a_0 = 11.6$ nm) and pore diameter ($D = 8.2$ nm) of the present SBA-15 sample, a layer thickness of 2.5 nm for the adsorbed surfactant film, and a cross-sectional radius of 2.5 nm for the cylindrical and wormlike geometries of the surfactant aggregates.

(i) When the surfactant forms surface micelles or adsorbed bilayer patches (Figure 1a), the volume-averaged configuration represents a surfactant layer at the pore wall. In the chosen silica contrast-match scenario, this geometry corresponds to a cylindrical shell. Hence, the form factor of a hollow cylinder, $P_{\text{HC}}(q)$, is used in eq 1. It causes changes in the individual Bragg peak intensities from the original lattice structure factor $S(q)$ (dotted) to the peak intensities indicated by shaded regions. Since the first minimum in $P_{\text{HC}}(q)$ is situated at a q value near the (10) Bragg reflection, the intensity of this peak is strongly reduced.

(ii) When the surfactant forms cylindrical micelles or related structures in the center of the pores (Figure 1b), this can be simulated by using the form factor of a cylindrical rod, $P_{\text{rod}}(q)$, in eq 1. As $P_{\text{rod}}(q)$ is a monotonically decreasing function in the

relevant q range, the intensity of the (10) Bragg peak is enhanced relative to the (11) and (20) peaks in this scattering geometry.

(iii) When the surfactant is excluded from the pore space and forms wormlike micelles in the extrapore liquid volume, no Bragg scattering occurs in the chosen contrast scenario. Figure 1c shows the scattering profile for wormlike micelles of the surfactant based on the form factor for semiflexible worms, $P_{\text{worm}}(q)$.¹⁶

In the experiments, the influence of surface modification on the morphology of the surfactant aggregates in the pores was studied by coadsorption of the amino acid lysine. The level of surface modification can be expressed by the relative adsorption level of lysine, $\theta = n^L/n_m^L$, where n^L is the amount of lysine adsorbed and n_m^L is the maximum adsorbed amount (corresponding to a surface density of lysine molecules of 0.45 nm^{-2}). Scattering curves for a fixed surfactant loading (95% of maximum adsorption, corresponding to $\varphi \approx 0.4$, where φ is the surfactant volume fraction in the pore space¹⁴) at different lysine adsorption levels ($\theta = 0.1, 0.7$, and 0.9) are shown in Figure 2. At the chosen lysine concentrations, the

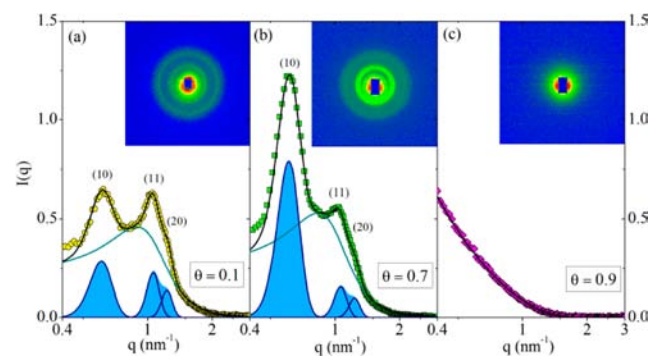


Figure 2. SANS 1D profiles $I(q)$ and (insets) 2D scattering patterns for SBA-15 slurry samples prepared with a fixed amount of C_{12}E_3 ($f = 0.95$) in contrast-matching $\text{H}_2\text{O}/\text{D}_2\text{O}$ at different degrees of surface modification with lysine: (a) $\theta = 0.1$; (b) $\theta = 0.7$; (c) $\theta = 0.9$. Also shown are fits to the scattering profiles (black lines) based on a combination of a diffuse scattering term I_{diff} (green lines) and a Bragg scattering term I_{Bragg} (contours of blue shaded areas). In (c), the data were fitted by the form factor for wormlike micelles, $P_{\text{worm}}(q)$,¹⁶ without the Bragg scattering term.

scattering originated almost entirely from the surfactant aggregates, while lysine made no detectable contribution. The scattering curves for $\theta = 0.1$ and 0.7 represent a superposition of Bragg scattering and diffuse scattering. These could be separated by modeling the diffuse scattering using the Teubner–Strey relation,¹⁷ which applies to microphase-separated systems with correlations among the domains. The resulting contributions $I_{\text{Bragg}}(q)$ and $I_{\text{diff}}(q)$ are also shown in the graphs. The results for the sample with the lowest lysine adsorption ($\theta = 0.1$; Figure 2a) are in close agreement with earlier results for a sample without lysine.¹³ As the lysine adsorption level was increased, the (10) Bragg peak strongly increased, as shown for the $\theta = 0.7$ sample (Figure 2b). However, as the lysine adsorption level was further increased to $\theta = 0.9$, the Bragg scattering vanished, and the profile could be modeled using $P_{\text{worm}}(q)$ ¹⁶ (Figure 2c). The pronounced changes in scattering behavior induced by surface modification can also be seen in the primary scattering patterns, which are shown as insets in Figure 2. Results such as those in Figure 2

were obtained independent of whether lysine was added before or after the surfactant, indicating that the morphology of the surfactant aggregates depends solely on the level of surface modification.

Further analysis of the data was performed on the basis of integrated intensities.¹⁴ Individual integrated Bragg peak intensities \tilde{I}_{hk} are shown in Figure 3a, and the overall

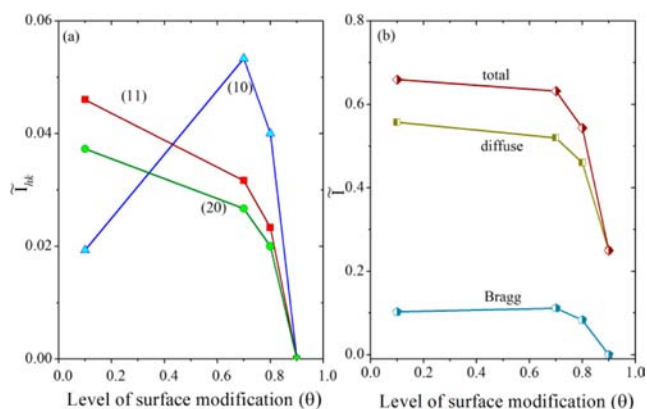


Figure 3. Integrated scattering intensities for the surfactant $C_{12}E_5$ in SBA-15 slurry samples as functions of θ : (a) individual integrated intensities of the three leading Bragg peaks; (b) overall contributions from Bragg and diffuse scattering and the total integral scattering intensity.

contributions from Bragg scattering (\tilde{I}_{Bragg}) and diffuse scattering (\tilde{I}_{diff}) are given in Figure 3b as functions of the level of surface modification θ . The total integrated intensity, $\tilde{I}_{\text{total}} = \tilde{I}_{\text{Bragg}} + \tilde{I}_{\text{diff}}$ which is also shown in Figure 3b, is a measure of the overall amount of surfactant in the samples. From the evolution of the individual peak intensities \tilde{I}_{hk} and the total intensity \tilde{I}_{total} shown in Figure 3, the following conclusions can be drawn:

(1) As the lysine surface concentration θ was increased from 0.1 to 0.7, the intensity \tilde{I}_{10} increased by a factor 3 while the intensities \tilde{I}_{11} and \tilde{I}_{20} decreased. This change in the peak intensities, combined with the fact that the amount of surfactant in the sample (as indicated by \tilde{I}_{total}) remained constant, is conclusive evidence for a change in the morphology of the aggregates in the pores from a surfactant layer at the pore walls (at $\theta = 0.1$) to aggregates with cylindrical geometry in the cores of the pores (at $\theta = 0.7$). The mean diameter (d) of these aggregates was estimated from the volume fraction of surfactant in the pores as $d = D\sqrt{\varphi}$. With $D = 8.2$ nm and $\varphi = 0.4$, this expression gives $d = 5.2$ nm, which is similar to the diameter of wormlike micelles of $C_{12}E_5$ in solution.¹⁸ This simple estimate implies that cylindrical micelles exist within the entire length of the cylindrical pores.

(2) As the lysine surface concentration was further increased from $\theta = 0.7$ to $\theta = 0.9$, all of the Bragg peaks vanished ($\tilde{I}_{\text{Bragg}} = 0$), indicating that no surfactant was left in the pore space, while \tilde{I}_{total} fell off to a low value, indicating that part of the surfactant was present in the extrapore liquid of the slurry sample (see Scheme 1), where the surfactant formed wormlike micelles, as can be concluded from the fit of the scattering curve in Figure 2c.

For nonionic surfactants such as $C_{12}E_5$, the dominant mechanism of binding to a silica surface is hydrogen bonding of the silanol groups to oxygen atoms of the ethoxylate head groups, either directly¹⁹ or mediated by water molecules.²⁰

When lysine competes with the surfactant for the silanol groups, the number of groups available for surfactant binding decreases, and thus, its adsorptive binding to the surface becomes weaker as θ increases. However, since lysine is adsorbed on the silica surface via its terminal amino group,²¹ the zwitterionic α -amino acid moiety is exposed to the pore space and may contribute to the binding of surfactant via N–H...O hydrogen bonds from the α -amino group at high lysine adsorption levels. Further studies to obtain a better understanding of the balance of attractive and repulsive interactions of the surfactant with the pore walls are underway.

To our knowledge, this work is the first to show that the partitioning of wormlike micelles between a bulk solution and nanopores can be controlled by tuning the surfactant–wall interactions. According to the seminal theoretical study on chain partitioning between a pore and a reservoir by Freed et al.,¹⁰ attractive polymer–surface interactions become decisive in the regime of strong confinement, where $Q \equiv (\pi R_G/L)^2 > 1$, in which R_G is the radius of gyration of the polymer and L is a measure of the pore size. The surfactant studied here, $C_{12}E_5$, forms semiflexible cylindrical micelles with a persistence length (l_p) of ca. 13 nm and a contour length (L_c) of 300 nm at 20 °C.¹⁸ Taking $R_G = (2l_p L_c) \approx 35$ nm and $L = D = 8.2$ nm, the present system corresponds to a confinement parameter $Q \approx 180$. For such high values of Q , the theory¹⁰ predicts a strong influence of the interaction parameter on the partition coefficient, decreasing from a high value for weakly attractive interactions to almost zero for weakly repulsive interactions (see Figure 9 in ref 10). This agrees with the observed transition in the partitioning of the cylindrical micelles of $C_{12}E_5$ when the level of surface modification increased from $\theta = 0.7$ to 0.9. Further studies will show whether the coadsorption method for controlling the partitioning of wormlike micelles between pores and bulk phases can also be applied to classical polymers with greater flexibility than the semiflexible micelles considered here.

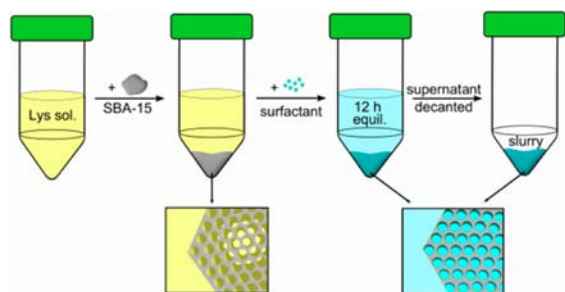
In conclusion, we have found that the self-assembly of a common nonionic surfactant in tubular 8 nm nanopores can be tuned by coadsorption of the amino acid lysine, which reduces the adsorption affinity for the surfactant. An evolution of equilibrium morphologies of the surfactant aggregates as a function of the level of surface modification θ was found using in situ SANS, which is free from artifacts that can arise during the drying process for electron microscopy. At low lysine adsorption levels, the surfactant formed patchy bilayer aggregates at the pore walls, as observed in the absence of lysine. At the highest degree of surface modification ($\theta = 0.9$), the surfactant was excluded from the pore space and formed wormlike micelles in the aqueous bulk phase, reminiscent of size exclusion of polymers from narrow pores with non-adsorbing walls. Remarkably, between these two regimes of weak and strong surface modification, we found a domain in which the surfactant could enter the pores and form cylindrical aggregates. We conjecture that this state of cylindrical micelles in tubular nanopores is stabilized by weak adsorptive interactions with the wall, which remain just strong enough to balance the loss in configurational entropy relative to wormlike micelles in the unconfined solution.

This work may trigger further in situ studies of morphological transitions of surfactant and polymer aggregates in nanoconfinement produced by precise tuning of their interactions with the pore walls. The results will also contribute to a fundamental understanding of the role of attractive and

repulsive interactions in the partitioning of polymeric entities between solution and nanopores.

Experimental Details. SBA-15 was synthesized as described previously²² and characterized by nitrogen adsorption and small-angle X-ray diffraction. The adsorption isotherm of lysine on SBA-15 was determined at pH 7 as reported previously¹⁵ and represented by the Langmuir equation (maximum specific adsorption $n_m^L = 0.57 \text{ mmol g}^{-1}$, adsorption constant $K^L = 1.0 \text{ mM}^{-1}$). The adsorption isotherm of the nonionic surfactant C₁₂E₅ in SBA-15 exhibited a pronounced sigmoidal shape, reaching a limiting adsorption n_m^s shortly above the critical micelle concentration ($\text{cmc} = 6.5 \times 10^{-5} \text{ M}$).¹³ For the present SBA-15 material, $n_m^s = 1.15 \text{ mmol g}^{-1}$. Samples for SANS measurements were prepared as sketched in Scheme 1 using a

Scheme 1. Sample Preparation for SANS Measurements^a



^aSBA-15 was added to solutions of lysine in a H₂O/D₂O mixture that matched the scattering length density of the silica. After surfactant addition and equilibration (12 h), the supernatant was removed. The resulting slurry samples consisted of SBA-15 powder containing most of the surfactant and an approximately equal volume of solution.

H₂O/D₂O solvent mixture that matched the scattering length density of SBA-15 ($\rho_{\text{silica}} = 3.7 \times 10^{-4} \text{ nm}^{-2}$).¹⁴ Samples with fixed surfactant loading (corresponding to a relative filling $f = n^s/n_m^s = 0.95$) and a range of lysine surface concentrations θ were prepared.

■ ASSOCIATED CONTENT

📄 Supporting Information

Characterization of SBA-15 silica, adsorption isotherm of lysine on SBA-15, and SANS results for surfactant surface aggregates in the pores of SBA-15 without surface modification by lysine. This material is available free of charge via the Internet at <http://pubs.acs.org>.

■ AUTHOR INFORMATION

Corresponding Author

findenegg@chem.tu-berlin.de

Notes

The authors declare no competing financial interest.

■ ACKNOWLEDGMENTS

SANS was performed at Instrument D16 at ILL (Grenoble, France) and supported by the European Commission under Program CP-CSA_INFRA-2008-1.1.1 no. 226507-NMI3. Financial support by the German Research Foundation (DFG) in the framework of IGRTG 1524 is also gratefully acknowledged.

■ REFERENCES

- (1) Ramanathan, M.; Kilbey, S. M., II; Ji, Q.; Hill, J. P.; Ariga, K. *J. Mater. Chem.* **2012**, *22*, 10389.
- (2) Shin, K.; Xiang, H.; Moon, S. I.; Kim, T.; McCarthy, T. J.; Russell, T. P. *Science* **2004**, *306*, 76.
- (3) Ma, M.; Titivesky, K.; Thomas, E. L.; Rutledge, G. C. *Nano Lett.* **2009**, *9*, 1678.
- (4) Yu, B.; Jin, Q.; Ding, D.; Li, B.; Shi, A.-S. *Macromolecules* **2008**, *41*, 4042.
- (5) Patra, N.; Král, P. *J. Am. Chem. Soc.* **2011**, *133*, 6146.
- (6) Angelikopoulos, P.; Bock, H. *J. Phys. Chem. Lett.* **2011**, *2*, 139.
- (7) Arai, N.; Yasuoka, K.; Zeng, X. C. *J. Am. Chem. Soc.* **2008**, *130*, 7916.
- (8) May, S.; Bohbot, Y.; Ben-Shaul, A. *J. Phys. Chem. B* **1997**, *101*, 8648.
- (9) de Gennes, P.-G. *Scaling Concepts in Polymer Physics*; Cornell University Press: Ithaca, NY, 1979.
- (10) Freed, K. F.; Dudowicz, J.; Stukalin, E. B.; Douglas, J. F. *J. Chem. Phys.* **2010**, *133*, No. 094901.
- (11) Zhao, D.; Feng, J.; Huo, Q.; Melosh, N.; Fredrickson, G. H.; Chmelka, B. F.; Stucky, G. D. *Science* **1998**, *279*, 548.
- (12) Sundblom, A.; Oliveira, C. L. P.; Pedersen, J. S.; Palmqvist, A. E. C. *J. Phys. Chem. C* **2010**, *114*, 3483.
- (13) Mütter, D.; Shin, T.; Demé, B.; Fratzl, P.; Paris, O.; Findenegg, G. H. *J. Phys. Chem. Lett.* **2010**, *1*, 1442.
- (14) Shin, T. G.; Mütter, D.; Meissner, J.; Paris, O.; Findenegg, G. H. *Langmuir* **2011**, *27*, 5252.
- (15) Bharti, B.; Meissner, J.; Gasser, U.; Findenegg, G. H. *Soft Matter* **2012**, *8*, 6573.
- (16) Kholodenko, A. L. *Macromolecules* **1993**, *26*, 4179.
- (17) (a) Teubner, M.; Strey, R. *J. Chem. Phys.* **1987**, *87*, 3195. (b) Sottmann, T.; Strey, R.; Chen, S.-H. *J. Chem. Phys.* **1997**, *106*, 6483.
- (18) Menge, U.; Lang, P.; Findenegg, G. H.; Strunz, P. *J. Phys. Chem. B* **2003**, *107*, 1316.
- (19) Trens, P.; Denoyel, R. *Langmuir* **1993**, *9*, 519.
- (20) Matsson, M. K.; Kronberg, B.; Claesson, P. M. *Langmuir* **2004**, *20*, 4051.
- (21) Kitadai, N.; Yokoyama, T.; Nakashima, S. *J. Colloid Interface Sci.* **2009**, *329*, 31.
- (22) Akcakayiran, D.; Mauder, D.; Hess, C.; Sievers, T. K.; Kurth, D. G.; Shenderovich, I.; Limbach, H.-H.; Findenegg, G. H. *J. Phys. Chem. B* **2008**, *112*, 14637.